Journal of Vibration Engineering & Technologies
https://doi.org/10.1007/s42417-024-01408-x

ORIGINAL PAPER

# A Novel Arrangement of Multiple Cylinders of Different Structural Conditions Dictating Wind Energy Harvesting at Very Low Reynolds Number

**Prasenjit Dey**[1]

Received: 22 February 2024 / Revised: 16 April 2024 / Accepted: 25 April 2024


## Abstract

**Purpose** Vortex-induced vibration (VIV) of a single cylinder is different from the multiple cylinders, and energy harvesting from the VIV of multiple cylinders by utilizing the piezoelectric technique is one of the promising techniques. The number of cylinders, spacing between them, and structural condition of the interference cylinder influence the fluid forces on the cylinders, and consequently, the efficiency of the harvested output power is affected.

**Method** A two-dimensional unsteady laminar flow condition is coupled with a spring-mass-damper system to analyze the fluid-structure interaction. The influence of multiple cylinders arranged in tandem on the flow characteristics and energy harvesting from VIV are investigated systematically in the present study. The number of cylinders is varied as $N = 1$, 2, 3, and 4 and the spacing between the tandem cylinders is varied as, $S^*$ ($S/D$, $D$ is the cylinder diameter) = 3, 6, 9. Also, a wide combination of fixed and/or freely vibrating structural conditions are considered. The incoming flow velocity of wind is kept very low as Reynolds number, $Re = 100$.

**Results and Conclusions** It is observed that, irrespective of the structural condition, critical value of $S^*$ is noticed at which there is no wake undulation. The strength of the vortex increases with increasing $S^*$, which is significantly dependent on the vibrational condition of the cylinders. The output power harvested from VIV is found to be considerably reliant on spacing as well as on the structural condition. A maximum harvested power of 10.55 mW is achieved at $S^* = 9$ and $N = 4$ in the present considered cases when all the cylinders are allowed to vibrate freely. The present results provide knowledge on the application of a set of tandem cylinders combining with vibrational mode for harvesting the power from VIV in a practically engineered nano/micro energy harvesting system, as demanded by the specific application on hand.

**Keywords** Four cylinders · Tandem · VIV · Energy harvesting · Piezoelectric

## List of Symbols

| | |
|---|---|
| $C$ | Damping coefficient |
| $C_D$ | Drag coefficient |
| $C_L$ | Lift coefficient |
| $D$ | Cylinder diameter, m |
| $f_{cycle}$ | Frequency of cylinder oscillation, Hz |
| $fn$ | Natural frequency, Hz |
| $K$ | Spring stiffness, N/m |
| $L$ | Length of cylinder, m |
| $L_d$ | Downstream length of domain, m |
| $L_u$ | Upstream length of domain, m |
| $M$ | Total mass of system, kg |
| $m$ | Actual mass of cylinder per unit length |
| $m^*$ | Non-dimensional mass of body, $\frac{4m}{\pi\rho D^2}$ |
| $N$ | Number of cylinders |
| $p$ | Pressure, N/m$^2$ |
| $Power_{VIV}$ | Energy harvested from VIV, Watt |
| $Re$ | Reynolds number, $\frac{\rho U_\infty D}{\mu}$ |
| $S$ | Centre to centre distance between cylinders, m |
| $S^*$ | Non-dimensional Spacing, - |
| $St$ | Strouhal number |
| $t$ | Time, s |
| $T_{cycle}$ | Time period of one complete cycle of oscillation, s |
| $t^*$ | Non-dimensional time, $\frac{t.U_\infty}{D}$ |
| $u$, $v$ | Velocity components in x and y directions, m/s |

✉ Prasenjit Dey
prasenjit.dey@nitgoa.ac.in

[1] Department of Mechanical Engineering, National Institute of Technology Goa, Cuncolim, Goa 403703, India

Published online: 14 May 2024

| | |
|---|---|
| $U_r$ | Reduced velocity, $\frac{U_\infty}{f_n D}$ |
| $U_\infty$ | Free stream velocity, m/s |
| $VIV$ | Vortex induced vibration |
| $x,y$ | Coordinates |
| $\ddot{y}$, $\dot{y}$ and $y$ | Transverse acceleration, velocity and displacement of body |
| $\rho$ | Density, kg/m$^3$ |
| $\mu$ | Dynamic viscosity, N.s/m$^2$ |
| $\zeta$ | Structural damping ratio |
| $\omega_{osc}$ | Angular velocity, rad/s |
| $\eta_{VIV}$ | Energy conversion efficiency |

## Introduction

In recent years, the development and demand for renewable energy technology have intensified due to increased concerns on non-renewable energy and its limited resources, as well as different environmental issues [1]. As a typical renewable energy, solar and wind energy have been acknowledged exceptionally by an incredible number of researchers in recent years throughout the world, as both of these energies are undoubtedly available all around the world with varying concentrations. However, apart from the solar and wind energy, wave energy has also great prospective for energy harvesting as the energy fluctuation is less than solar and wind power [2].

One of the many small scale energy harvesting techniques, the piezoelectric energy harvesting method gains more attention due to its enormous advantages, such as sustainability, eco-friendly, moderately compact size, and efficiency to generate small scale energy to run low-power electronics devices [3, 4]. As the wind energy is extensively available and the structure of a wind energy harvesting device with a small piezoelectric strip is simple with a high output voltage, a large number of research is being carried out on piezoelectric energy harvesters [5, 6]. Several techniques are being used in the piezoelectric wind energy harvesting system, viz., vortex-induced vibration (VIV), flutter, and galloping energy harvesters [7, 8].

Wind energy harvesting is mainly done by the application of wind-induced vibration using bluff bodies or other kinds of structures that can convert wind energy into mechanical vibration energy. Energy harvesting or the conversion of energy significantly depends on the fluid flow characteristics and the corresponding heat transfer behaviour [9–14]. The cylinder type bluff bodies can efficiently harvest electric energy from wind energy using the VIV technique at a low wind speed [15–19]. Liu et al. [17] investigated the VIV-based wind energy harvesting by a cylinder, and found that the output voltage can increase from less than 2 V to more than 10 V in the wind speed range of 2.5–5 m/s when the double plates are placed at upstream of the cylinder. For efficient VIV energy harvesting from low wind speeds of $<2$ m/s, a cylindrical bluff body should be aligned with the piezoelectric beam, and a maximum average power of 30 μW can be achieved from that arrangement with a load resistance of 800 kΩ [15]. Three types of cross sections of a bluff body, circular, triangular, and semi-circular were investigated for low velocity of water flow energy harvesting by Sun et al. [18]. It is observed that a maximum power density of 1.949 mW/cm$^3$ can be harvested at a flow velocity of 0.48 m/s. However, due to its self-excitation, and self-restriction, impact of VIV on energy harvesting is less compared to galloping and fluttering [20, 21]. Although, a large number of numerical and experimental studies have been accomplished till date using different transduction techniques, viz., vibration [21–24], piezoelectric [25, 26], electromagnetic [27–29], and electrostatic [30, 31]. Nevertheless, the efficiency of energy conversion by using VIV is quite low due to a small bandwidth of the synchronization (lock-in) region [32]. However, the output power from wind energy harvesting needs to be improved for a large range of wind speeds, and to do so, several methods such as the shape of the bluff bodies, length of the piezoelectric sheet, cylinder's tip mass, stiffness, and mass of damping system have been endeavoured [17, 33–35]. A numerical analysis of energy harvesting from VIV using a circular cylinder is investigated within the range of $Re$, $96 \leq Re \leq 118$ and results revealed that the harvested power along with voltage output is promisingly effected by the load resistance [36]. Furthermore, the harvested energy from VIV of a cylinder can be enhanced by attaching extra cylindrical rods or by changing the cylinder geometry [37, 38]. Along with these techniques, multi-cylinder arrangement is found to be a resourceful technique to improve the power harvested from VIV [39–42]. The wake developed by the upstream cylinder produces a large VIV amplitude on the downstream cylinder when the spacing between them is less than $35D$ [38], and accordingly, a large amount of lift force is experienced by the downstream cylinder, resulting in an improvement in output power [42]. The influence of cylinder diameters and spacing between two tandem cylinders is found to be prominent and the fluid forces are very sensitive to diameter and spacing, with a maximum power conversion efficiency of 88.6% of the Betz limit at flow speed of 1.08 m/s with cylinder spacing 2.5–5.0D [39]. Consequently, it can be noticed that the flow characteristic and vortex phenomenon are different for the freely vibrating cylinder than the fixed one [43]. A very recent study depicted that an interference cylinder can enhance the energy generation of a single bluff body piezoelectric energy harvester by an amount of 624% compared to that of without an interference cylinder [44].

It can be noticed from the foregoing studies that multiple cylinders are more efficient in energy harvesting from

**Table 1** Summary of previous studies on energy harvesting from VIV of multi-cylinders

| Author (s) | No. of cylinders | Style of arrangement | Structural condition |
|---|---|---|---|
| Hobbs and Hu [45] | 4 | Tandem | Freely vibrating |
| Kim and Bernitsas [39] | 1, 2, 3, 4 | Tandem | Freely vibrating |
| Shan et al. [46] | 2 | Tandem | Freely vibrating |
| Zhang et al. [41] | 2 | Tandem | Freely vibrating |
| Zhang et al. [47] | 2 | Tandem | Downstream cylinder-fixed |
| Sun et al. [48] | 2 | Tandem | Freely vibrating |
| Zhang et al. [40] | 4 | Staggered | Freely vibrating |
| Ding et al. [23] | 3 | Tandem | Freely vibrating |
| Zhang et al. [21] | 2 | Tandem | Downstream cylinder-fixed |
| Hu et al. [49] | 3 | Tandem | Freely vibrating |
| Han et al. [50] | 3 | Equilateral Triangular | Freely vibrating |
| Chen et al. [51] | 2 | Tandem | Upstream cylinder-fixed |
| Tamimi et al. [52] | 2 | Tandem | Freely vibrating |

VIV than a single cylinder. A number of available studies related to VIV of single or multi cylinders are summarized in Table 1. It is pertinent from Table 1 that most of the studies were for two or three cylinders, and very few studies are available for four cylinders that are also allowed to vibrate freely. As mentioned earlier, the space, number of cylinders, and structural condition of the interference cylinder influence the fluid forces on the cylinders, and consequently, the efficiency of the harvested output power is affected. Although, few questions are remained unanswered to date. Are multiple cylinders always needed to allow vibrate freely for maximum energy harvesting? What are the effects of the static and vibrating conditions of cylinders on the flow characteristics and the corresponding energy harvesting? What are the detailed comparisons of flow phenomena and energy harvested from VIV between single and multi-cylinders arrangements at very low $Re = 100$? Can the overall energy harvesting from VIV always be increased by increasing the number of multi-cylinders, and the spacing between them?

Thus, the present work aims to explore the flow characteristics around the four cylinders organised in tandem at different spacings with different structural combinations of static and freely vibrating conditions, and their corresponding effect on the energy harvesting from VIV to address the above mentioned issues. In addition, the influence of the number of cylinders ($N$) is also investigated for an overall understanding of flow behaviour and energy harvesting for different cylinder arrangements. For this, four different values of $N$ are considered as; $N = 1$, 2, 3 and 4 with cylinder diameter, $D$ for different spacing, $S/D = 3$, 6, and 9 at very low Reynolds number, $Re = 100$. The structural conditions; static and freely vibrating states are varied, and different combinations are taken into account at the same time. The stream lines, vorticity, lift-coefficient, transverse displacement of the vibrating cylinder, frequency of transverse oscillation, energy harvested, and energy conversion efficiency are calculated and are considered for the detailed comparison.

The rest of the present study is prepared as follows: Sect. "Problem description" covers the problem description, including the numerical domain and different cases of present analysis; Sect. "Governing equations and numerical methods" discusses governing equations and numerical methods, including the grid independency study and numerical validation. The present results, including the fluid flow characteristics of single and multi-cylinder arrangements and their impact on the energy harvesting, are thoroughly discussed in Sect. "Results and Discussions", whereas the concluding remarks are summarized in Sect. “Conclusion”.

## Problem Description

A combination of multiple cylinders of the same size of diameter, $D$, is placed in a tandem arrangement in a rectangular computational domain. A combination of one, two, three, and four circular cylinders is considered for the present numerical analysis of energy harvesting from Vortex Induced Vibration (VIV). Figure 1 depicts the schematic representation of the four cylinders configuration in a tandem arrangement. Two structural conditions of a cylinder are considered as static ($S$) and vibrating ($V$). The different conditions of multiple cylinder arrangements considered in the present numerical analysis are summarized in Tables 2, 3, and 4 for two, three, and four cylinders arrangement respectively. Each numerical case is characterized by the number of tandem cylinders, the space between the cylinders, and its motion; static or vibrating. The vibrating cylinder is spring and damper mounted and allowed to oscillate in the transverse direction only. The spring-damper arrangement is characterized by the spring stiffness of the spring, $K$, and the damping coefficient of damper, $C$ respectively.

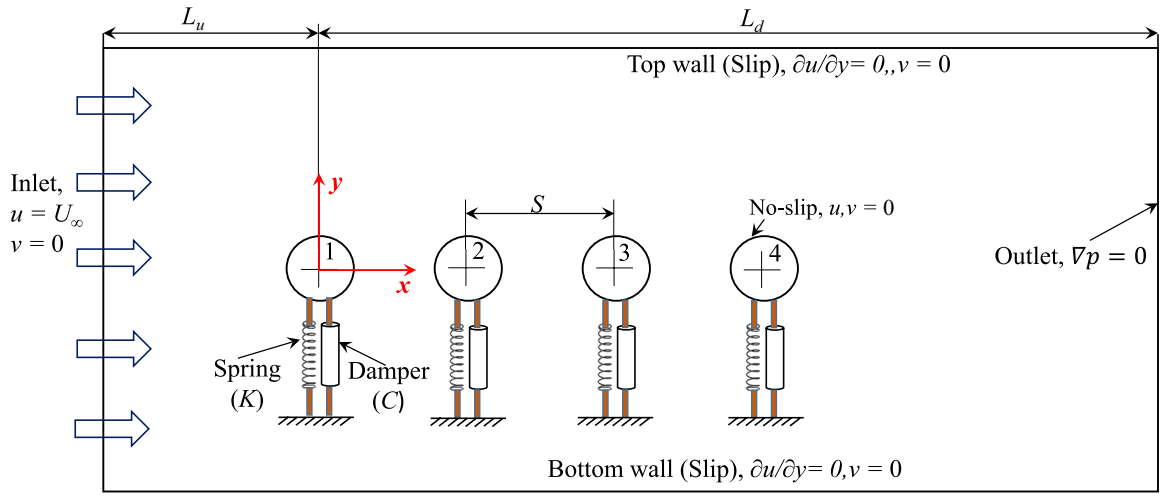


**Fig. 1** Schematic representation of the present numerical model

**Table 2** Details of different cases considered in the present numerical analysis of two cylinders arranged in tandem for varying space and structural combinations

| Case no. | Space | Cylinder 1 | | Cylinder 2 | |
|---|---|---|---|---|---|
| | | Static | Vibrating | Static | Vibrating |
| *2NxS-1* | 3*D*, 6*D*, and 9*D* | ***Y*** | *N* | *N* | ***Y*** |
| *2NxS-2* | *x* = 3, 6 and 9 | *N* | ***Y*** | ***Y*** | *N* |
| *2NxS-3* | | *N* | ***Y*** | *N* | ***Y*** |

*Y* yes; *N* no

The cylinder diameter, $D$ is preferred as the characteristic length to represent all the length quantities and Reynolds number, $Re$. In the numerical domain, the Cartesian coordinate is kept stationary. The boundary conditions associated with the present numerical analysis are also depicted in the Fig. 1. The origin of the coordinate system is located at the center of the first cylinder. The distances of the upstream (inlet) and downstream (outlet) boundaries from the origin of the coordinate system are denoted by $L_u$ and $L_d$, respectively. In the present study, the value of $L_u$ and $L_d$ is considered as $10D$, and $(N-1) \times S + 40D$, respectively. Where,

**Table 3** Details of different cases considered in the present numerical analysis of three cylinders arranged in tandem for varying space and structural combinations

| Case no. | Space | Cylinder 1 | | Cylinder 2 | | Cylinder 3 | |
|---|---|---|---|---|---|---|---|
| | | Static | Vibrating | Static | Vibrating | Static | Vibrating |
| *3N6S-1* | 6*D* | ***Y*** | *N* | *N* | ***Y*** | *N* | ***Y*** |
| *3N6S-2* | | *N* | ***Y*** | ***Y*** | *N* | *N* | ***Y*** |
| *3N6S-3* | | *N* | ***Y*** | *N* | ***Y*** | ***Y*** | *N* |
| *3N6S-4* | | *N* | ***Y*** | *N* | ***Y*** | *N* | ***Y*** |
| *3N6S-5* | | ***Y*** | *N* | *N* | ***Y*** | ***Y*** | *N* |
| *3N9S-1* | 9*D* | *N* | ***Y*** | *N* | ***Y*** | *N* | ***Y*** |

*Y* yes; *N* no

**Table 4** Details of different cases considered in the present numerical analysis of four cylinders arranged in tandem for varying space and structural combinations

| Case no. | Space | Cylinder 1 | | Cylinder 2 | | Cylinder 3 | | Cylinder 4 | |
|---|---|---|---|---|---|---|---|---|---|
| | | Static | Vibrating | Static | Vibrating | Static | Vibrating | Static | Vibrating |
| *4N6S-1* | 6*D* | *N* | ***Y*** | *N* | ***Y*** | *N* | ***Y*** | *N* | ***Y*** |
| *4N6S-2* | | *N* | ***Y*** | ***Y*** | *N* | *N* | ***Y*** | ***Y*** | *N* |
| *4N6S-3* | | ***Y*** | *N* | *N* | ***Y*** | ***Y*** | *N* | *N* | ***Y*** |
| *4N9S-1* | 9*D* | *N* | ***Y*** | *N* | ***Y*** | *N* | ***Y*** | *N* | ***Y*** |

*Y* yes; *N* no

$N$ is the number of cylinders and $S$ is the center to center distance between two tandem cylinders. The space between two consecutive cylinders, $S$ is varied as $3D$, $6D$ and $9D$. The top and bottom boundaries are symmetrically placed each $10D$ away from the center of the coordinate system, provides a blockage ratio of 0.05 [53].

## Governing Equations and Numerical Methods

### Equation of Flow

In the present work, the flow around the multiple cylinders is numerically investigated using a two-dimensional, laminar, unsteady, and incompressible flow equations. The governing equations are the continuity and Navier–Stokes equations which can be written in dimensional form as follows,

$$\nabla .u = 0 \tag{1}$$

$$\frac{\partial u}{\partial t} + u.\nabla u = -\frac{\nabla p}{\rho} + \frac{\mu}{\rho}(\nabla^2 u) \tag{2}$$

where $u = f(u,v)$ is the velocity field, $p$ is the static pressure and $t$ is the time. Here, $\rho$ is the density and $\mu$ is viscosity of the fluid.

The fluid properties of the flowing air are dependent on the Reynolds number, $Re$ and is defined as follows,

$$Re = \frac{\rho U_\infty D}{\mu} \tag{3}$$

The different fluid forces *i.e.* drag and lift are evaluated by using the viscous and pressure forces acting on the cylinder surfaces.

The drag force is calculated as follows,

$$F_D = 0.5 C_D \rho U_\infty^2 D \tag{4}$$

where $C_D$ is the drag coefficient.

The force exerted on the cylinder by the periodic fluctuations of flow is characterized by the lift force and is given by,

$$F_L = 0.5 C_L \rho U_\infty^2 D \tag{5}$$

where $C_L$ is the lift coefficient.

The flow at the inlet is set uniform, $u = U_\infty$ and $v = 0$. At the outlet, pressure outlet boundary condition is applied as $\nabla p = 0$. Slip boundary condition ($\partial u/\partial y = 0$, $v = 0$) is imposed for the lateral boundaries. No-slip boundary condition ($u = 0$, $v = 0$) is applied at the cylinder surfaces for the stationary cylinder and $u = 0$, $v = \dot{y}$ for the vibrating cylinder.

### Equation of Cylinder Motion

When the fluid flows over a solid body, it develops unsteady forces as well as moments around the surface of the body. As a result, the body may experience motion. The present numerical investigation aims to study the characteristics of free vibration in flexibly mounted circular cylinders arranged in tandem. The dynamics of the cylinders due to fluid forces is characterized by a combined mass-spring-damper system (refer Fig. 1). The equation of motion in the y-direction with one degree of freedom is given as [54];

$$M\ddot{y} + C\dot{y} + Ky = F_{total,y}(t) \tag{6}$$

where, $M$ is the total mass of the cylinder, $K$ is the spring stiffness, $C$ is the damping coefficient, $y$ is the transverse displacement of the oscillating cylinder; $F_{total,y}$ is the total force acting in the $y$-direction due to inertial, pressure and viscous force.

The non-dimensional form of the transverse motion equation can be written in the following form [55],

$$\ddot{Y} + (4\pi F_N \zeta)\dot{Y} + (2\pi F_N)^2 Y = \frac{2C_L}{\pi m^*} \tag{7}$$

where, $F_N$ ($=f_n \mathrm{D}/U_\infty, f_n =$ Natural frequency) is the normalized natural frequency of vibrating cylinder, $\zeta$ is the structural damping ratio, $m^* \left(= \frac{4m}{\pi \rho D^2}\right)$ is the non-dimensional mass of the body, where $m$ is the actual mass of the cylinder per unit length and $\rho$ is the density of the fluid, and $C_L$ is the instantaneous lift coefficients of the cylinder induced by VIV. The free-stream flow is assumed to be along the $x$-axis. $\ddot{Y}$, $\dot{Y}$, and $Y$ denote the normalized transverse acceleration, velocity, and displacement of the body, respectively. In the present numerical study, the structural damping ratio is set equal to zero ($\zeta = 0$) to allow maximum amplitude oscillations, and $m^*$ is set equal to 10 [56].

### Energy Harvesting System and Formulation

The electrical equivalent circuit to harvest wind energy from VIV using multiple piezoelectric sheets, along with the block diagram of the system, is shown in Fig. 2. The energy harvesting system consists of multiple piezoelectric beams to generate electricity from vibration, a rectifier, a DC-DC converter, an energy storage device, and a load.

The transverse motion of a vibrating cylinder induced by VIV when fluid flows over the cylinder can be utilized to harvest energy from the motion by using rack-pinion arrangements, electro-magnetism, and piezoelectric beams as discussed earlier. Here, an arrangement of multiple piezoelectric beams for energy harvesting from VIV is

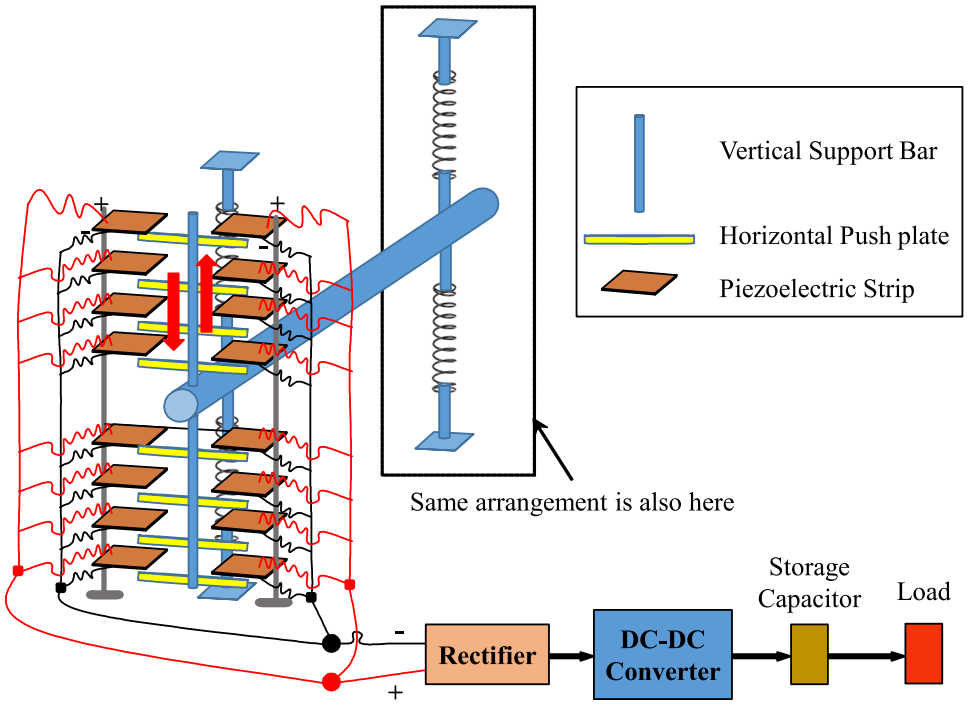


**Fig. 2** Elementary block diagram of energy harvesting system from VIV using piezoelectric

discussed. The total vortex induced motion converted to the power of the cylinder in one cycle is expressed as,

$$Power_{VIV} = \frac{1}{T_{cycle}} \int_0^{T_{cycle}} F_{total,y} \dot{y} dt \tag{8}$$

where, $T_{cycle}$ is the time period of one complete cycle of oscillation of freely vibrating cylinder and is defined as,

$$T_{cycle} = \frac{1}{f_{cycle}} = \frac{2\pi}{\omega_{osc}} \tag{9}$$

where, $f_{cycle}$ is the frequency of the cylinder oscillation in transverse direction and $\omega_{osc}$ is the angular Velocity of a sinusoidal oscillation.

Using Eq. 6, the Eq. 8 can be written as,

$$Power_{VIV} = \frac{1}{T_{cycle}} \int_0^{T_{cycle}} (M\ddot{y} + C\dot{y} + Ky)\dot{y} dt \tag{10}$$

Then finally, the efficiency of total energy conversion, $\eta_{VIV}$ is calculated as [2, 51, 54];

$$\eta_{VIV} = \frac{Power_{VIV}}{Power_{fluid} \times BetzLimit} \times 100\% \tag{11}$$

where $Power_{fluid}$ is the fluid power available in the fluid that flows over the cylinder, and according to Bernoulli's equation, it is calculated as,

$$Power_{fluid} = \frac{1}{2} \rho U_{\infty}^2 \left(D + 2y_{max}\right) L \tag{12}$$

Here $y_{max}$ is the maximum vibration amplitude and $L$ is the length of cylinder, which is set as unity in the two-dimensional simulations.

*Betz Limit* is the theoretical maximum efficiency that can be harnessed from the wind or water in flow. The value of it considered as 16/27 (=0.593), and is known as *Betz Limit* coefficient [2, 51, 54].

## Numerical Methods

The numerical analysis is carried out in a commercial Finite Volume Method based solver ANSYS Fluent to solve the unsteady, incompressible governing equations. The laminar viscous model is considered to represent the low Reynolds number flow condition. The pressure-correction-based iterative algorithm SIMPLE (semi-implicit method for pressure linked equations) is employed for the coupling between the velocity and pressure fields [57]. The STANDARD scheme is adopted to discretize the pressure term, while the power-law scheme is used to discretize the momentum equations. A first-order implicit formulation is adopted for the time discretization due to its unconditional stability and compatibility with the dynamic mesh [58]. The solution is considered to be converged once the residuals reach $10^{-6}$ for the continuity and momentum equations.

The motion of the cylinders induced by the VIV is modelled by the dynamic mesh scheme in the present study. The

movable boundaries, and/or bodies are progressed during the numerical simulation by the dynamic mesh model, and accordingly, the corresponding adjacent boundary mesh is adjusted. A UDF (User Defined Function) is embedded into the solver for computing the motion of the oscillating cylinders. At each time step, (i) the deformation of the domain is taken care of by the dynamic meshing tool, and the mesh is updated using the Laplace smoothing method, and (ii) the lift force on the cylinder is calculated by solving the Eqs. 1, 2, and 5. The lift force is then used in Eq. 7 to solve the transverse motion equation in the UDF.

## Grid Independence Study and Model Validation

For a numerical study, a minimum number of grids in the computational domain are required to obtain considerable accurate results with the least computational time. For this purpose, a comprehensive grid independence study is required to perform before analysing the all cases. Figure 3 shows the quadrilateral grid distribution for two circular cylinders arranged in tandem, separated by a distance, $S^* = 6$. A similar structured grid distribution is adopted in the present study for all the considered cases. A square region of size $2.5D \times 2.5D$ around the cylinder is generated to enclose the vibrating cylinder and is shown in Fig. 3 (left bottom view). As a result, the outer boundary of the enclosure square region is separated by four interface lines (red dash lines) from the moving and stationary regions. This square region moves along with the vibrating cylinder, and adjacent top and bottom domains are adopted as deforming zones to adjust the mesh.

The finest mesh is developed in the central block, which encloses the cylinder to effectively capture the wake wall interactions in both directions, and the grids become finer non-uniformly in the direction normal to the square block. The spacing between the first level of the grid and the cylinder wall is fixed at $0.005D$ for an adequate resolution of the boundary layer. Then the grid spacing linearly increases to a value of $0.01D$ within the central square region. After that, the grid size is increased to a maximum value of $0.1D$ with an expansion rate of 1.05 in the normal direction. The same spacing and expansion factor are used in all the considered cases, resulting in an increment in the number of cells with the increasing number of cylinders.

At first, grid and time-step sensitivity tests are conducted to further analyse an extensive number of cases. As the primary goal is to investigate the effect of the number of cylinders on the VIV and its corresponding energy harvesting, thus two freely vibrating cylinders arranged in tandem at a spacing, $S^* = 6$ and $Re = 100$ is considered for the sensitivity

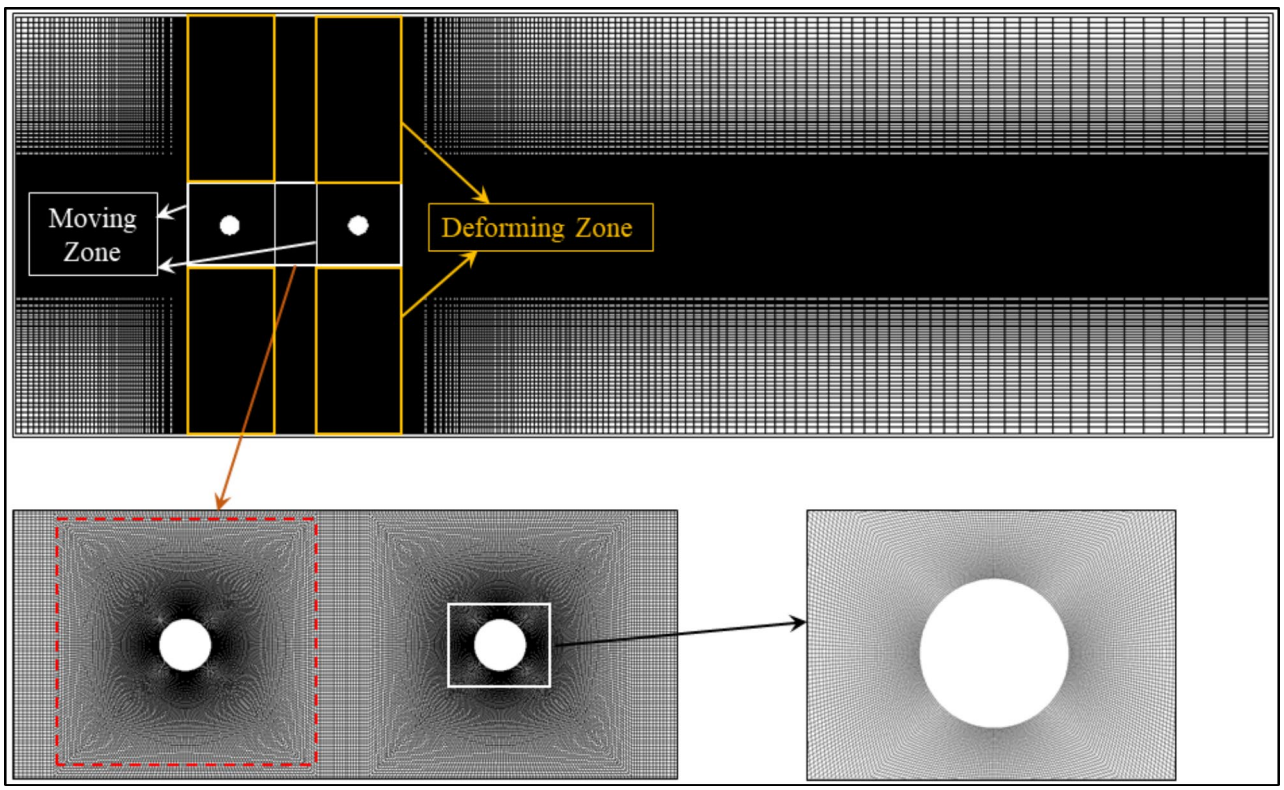


**Fig. 3** Local grids distribution within the whole computational domain. Also, grids around the multiple cylinders along with zoomed view of grids around a cylinder is depicted

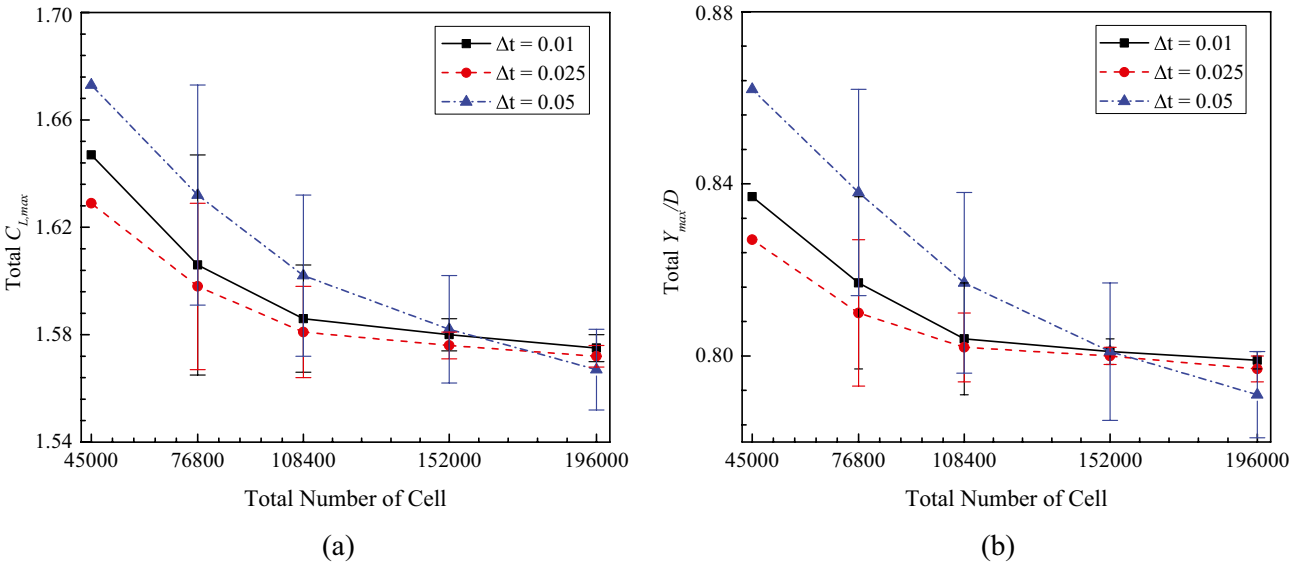


**Fig. 4** Details of grid and time-step sensitivity test on (a) Total $C_{L,max}$ and (b) Total $Y_{max}/D$

test. A total of five different mesh sizes, along with three different time-steps, are adopted for the independency study. Two different quantitative data, viz., total maximum lift coefficient ($C_{L,max}$), and total normalized maximum cylinder displacement ($y_{max}/D$), is selected for comparing different mesh sizes at different time steps. The detailed study of grid and time-step sensitivity test on $C_{L,max}$ and $Y_{max}/D$ is shown in Fig. 4. The percentage deviation in between the two corresponding grids is also shown in the figure as error bar. It is observed that the percentage deviation of total $C_{L,max}$, and total $y_{max}/D$ between the two grid sizes, 1,08,400 and 1,52,000, is 0.324 and 0.344, respectively, for time step 0.025 and 0.353 and 0.387, respectively for time step 0.01. However, with a further increment of grid size to 1,96,000; the percentage deviation is found to be insignificant. In addition, the percentage deviation of total $C_{L,max}$, and total $y_{max}/D$ between two time steps, 0.025 and 0.01 is 0.294 and 0.255 respectively, for grids 1,08,400. However, this percentage deviation between time steps 0.025 and 0.05 is 1.294 and 1.854, respectively. Thus, in the present numerical analysis, a grid size of 1,08,400 and a time step of 0.025 is considered for simulation of all the cases to reduce the computation cost with considerable accuracy.

In order to examine the accuracy and consistency, the numerical results are compared with some benchmark results for a single vibrating circular cylinder in the range of reduced velocity $\left(U_r = \frac{U_\infty}{f_n D}\right)$, $2 \le U_r \le 10$, $m^* = 10$, $\zeta = 0$ and $Re = 100$. The discrepancy of the r.m.s lift coefficient ($C_{L,rms}$) and maximum normalized transverse displacement ($y_{max}/D$) of the vibrating cylinder calculated from the present numerical analysis with the published results [59, 60] are shown in Fig. 5. It can be observed from the Fig. 5 that both the quantitative parameters are in close agreement with the data reported in the previous studies with a maximum error of 4.5%.

## Results and Discussions

A two-dimensional, laminar, unsteady, and incompressible fluid flows over a single and/or multiple circular cylinders and develops a transverse oscillation motion on the vibrating cylinder induced by VIV. As the present study mainly focuses on the multi cylinder arrangements, however, the detailed analysis of fluid flow and its effect on the energy harvesting from VIV for a single cylinder is also presented in the study in Appendix – A. It is found that the maximum power developed from VIV is found as 2.53 mW at $U_r = 5$ within the considered cases of a single vibrating cylinder in the present study. The present numerical investigation is further focussed on multi cylinder arrangement at variable spacing between the cylinders, and for different combinations of static and vibrating conditions for each cylinder at $Re = 100$, $U_r = 5$, $m^* = 10$, and $\zeta = 0$. The following sections describe the VIV response and corresponding power harvesting from VIV of single, two, three, and four circular cylinders arranged in tandem, respectively, and a detailed comparison between each considered case.

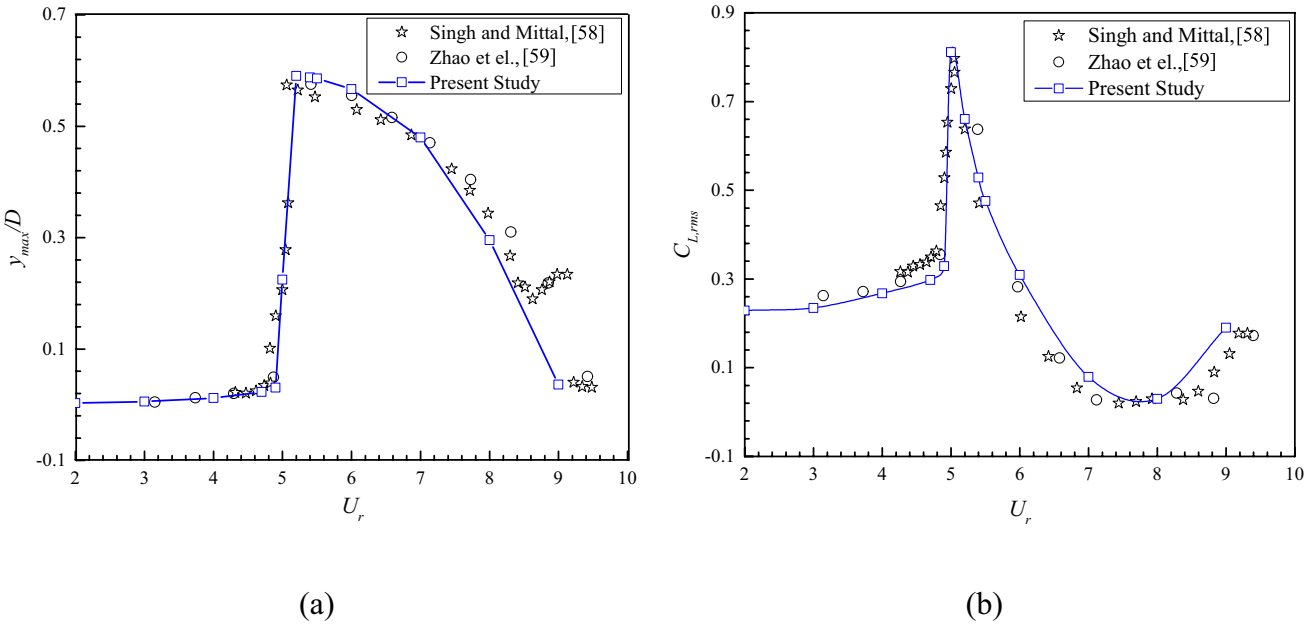


**Fig. 5** Validation of the present numerical results for single vibrating circular cylinder (a) of $y_{max}/D$ and (b) $C_{L,rms}$

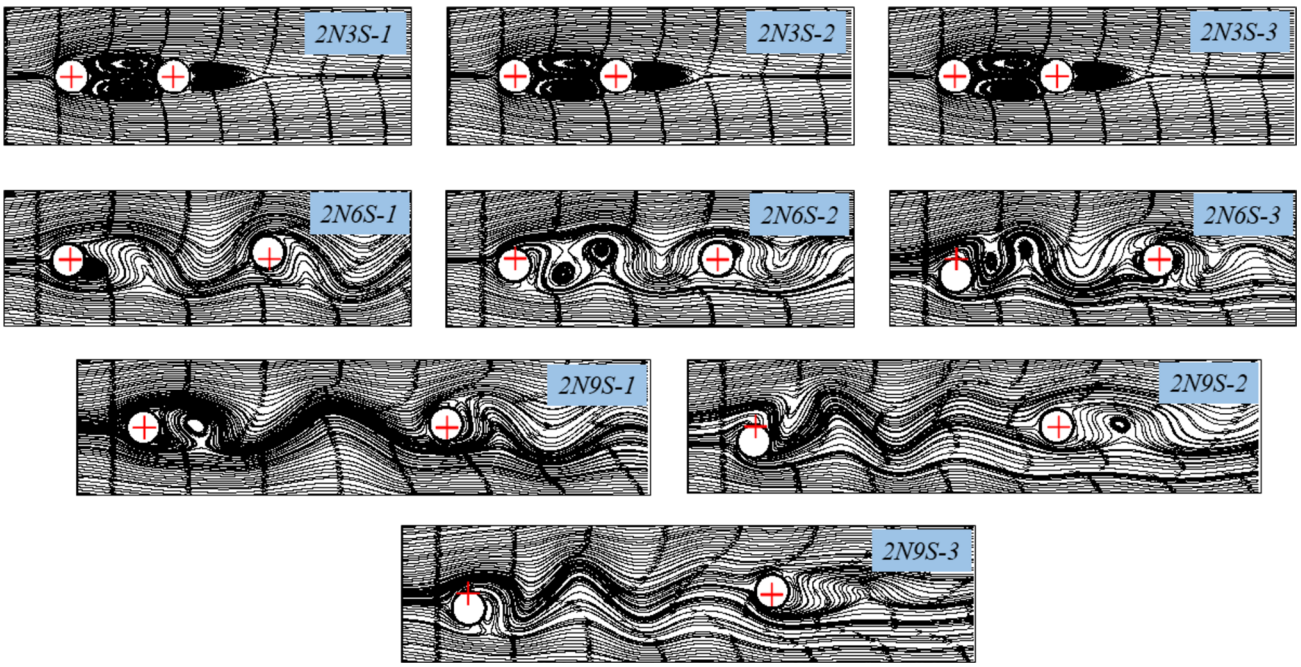


**Fig. 6** Instantaneous ($t^*=250$) streamline pattern for different space and different structural combinations at $U_r=5$, $m.^*=10$ and $Re=100$

## Streamline Characteristics

The flow pattern of fluid flowing over a body can be easily understood by analysing the streamline pattern and vorticity contour. Figures 6 and 7 depict the instantaneous streamline pattern when fluid flows over multiple cylinders, $N=2$ and 4, respectively, at $U_r=5$, $m^*=10$, $\zeta=0$ and $Re=100$. Three different values of space between the cylinders are considered as $S^*=3$, 6 and 9, and the corresponding cases are summarized in Table 2.

Figure 6 illustrates the instantaneous streamline pattern of fluid flow over the two cylinders at different values of

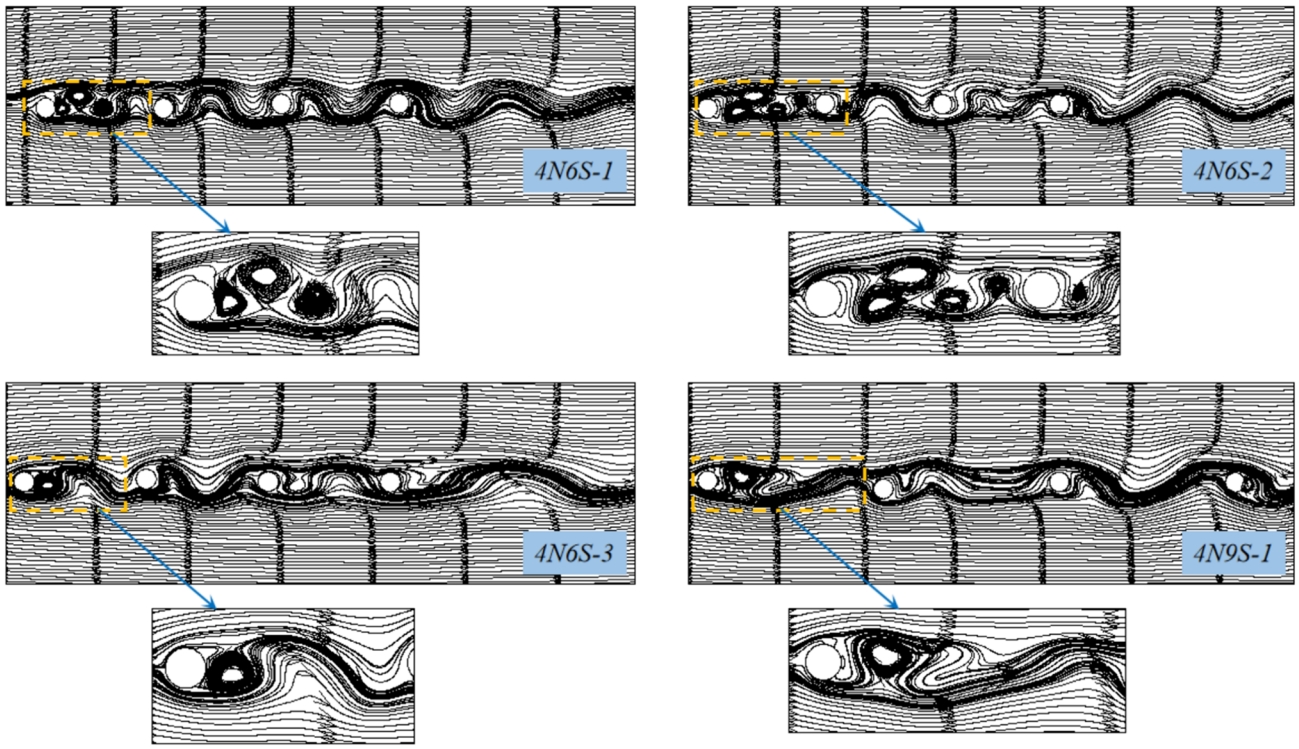


**Fig. 7** Instantaneous ($t^*=250$) streamline pattern for different space and different structural combinations at $U_r=5$, $m.^*=10$ and $Re=100$ and $N=4$

$S^*$. The flow behaviour in the locality of both the circular cylinders exhibits a very discrete nature for different values of the inter-cylinder spacing. When $S^*=3$, the wake formed by virtue of the boundary layer separation behind the first cylinder reattaches at the surface of the second cylinder for all the cases considered. The wake formed behind the second cylinder is symmetric by reattaching at a certain point from the rear stagnation point of the same cylinder. This streamline pattern signifies the steady behaviour of the flow around the two cylinders at $S^*=3$ irrespective of its structural conditions. It is also noted that the width of the standing recirculation regimes, or the wake of the upstream cylinder, is larger than the width of the wake of downstream cylinder. This wake characteristic implies that the more pressure drag is associated on the upstream cylinder than the downstream cylinder [61]. When $S^*=6$, the wake becomes wavy, and no reattachment is observed behind both cylinders. The wake formed behind the upstream cylinder stretches along the flow and streams over the downstream cylinder. However, a substantial amount of fluid that initially streamed over the upstream cylinder now flows over the top of the downstream cylinder. This phenomenon of fluid flow produces a significant enhancement in the lift force on the downstream cylinder compared to the upstream cylinder. For $S^*=9$, undulation of the streamline in all the considered cases is observed, however the wake developed behind the upstream cylinder is less wavy before contacting the downstream cylinder when the upstream cylinder is vibrating (refer to cases *2N9S-2* and *2N9S-3*).

Figure 7 depicts the instantaneous streamline pattern for the four cylinders arranged in tandem for $m^*=10$, $U_r=5$, $\zeta=0$ and $Re=100$. Here, only two values of non-dimensional spacing are considered as $S^*=6$ and 9. The primary reason for selecting such cases are as discussed earlier for the two and three tandem cylinder cases, that the total vibration of all the cylinders is found to be maximum at $S^*=6$ and 9. However, at $S^*=9$, the total vibration is greater when all the cylinders are allowed to vibrate freely. Thus, a single structural condition is considered to analyze the VIV of the four cylinders at $S^*=9$. A very unique characteristic of streamlines is observed for the flow over four cylinders arranged in tandem at $Re=100$. There are single to four wakes observed in between the Cyl-I and Cyl-II for the different structural conditions and spacing. It can be noticed that the wake is wavy behind each and every cylinders for all the considered cases. However, the characteristics of the wake structures are different for every case depending on the structural conditions of the cylinders and spacing. At $S^*=6$ and when all the cylinders are allowed to vibrate freely (*4N6S-1*), three wakes are observed behind the Cyl-I. Although, at $S^*=9$ and for all the vibrating cylinders (*4N9S-1*), only one wake is noticed with stretched in nature. When

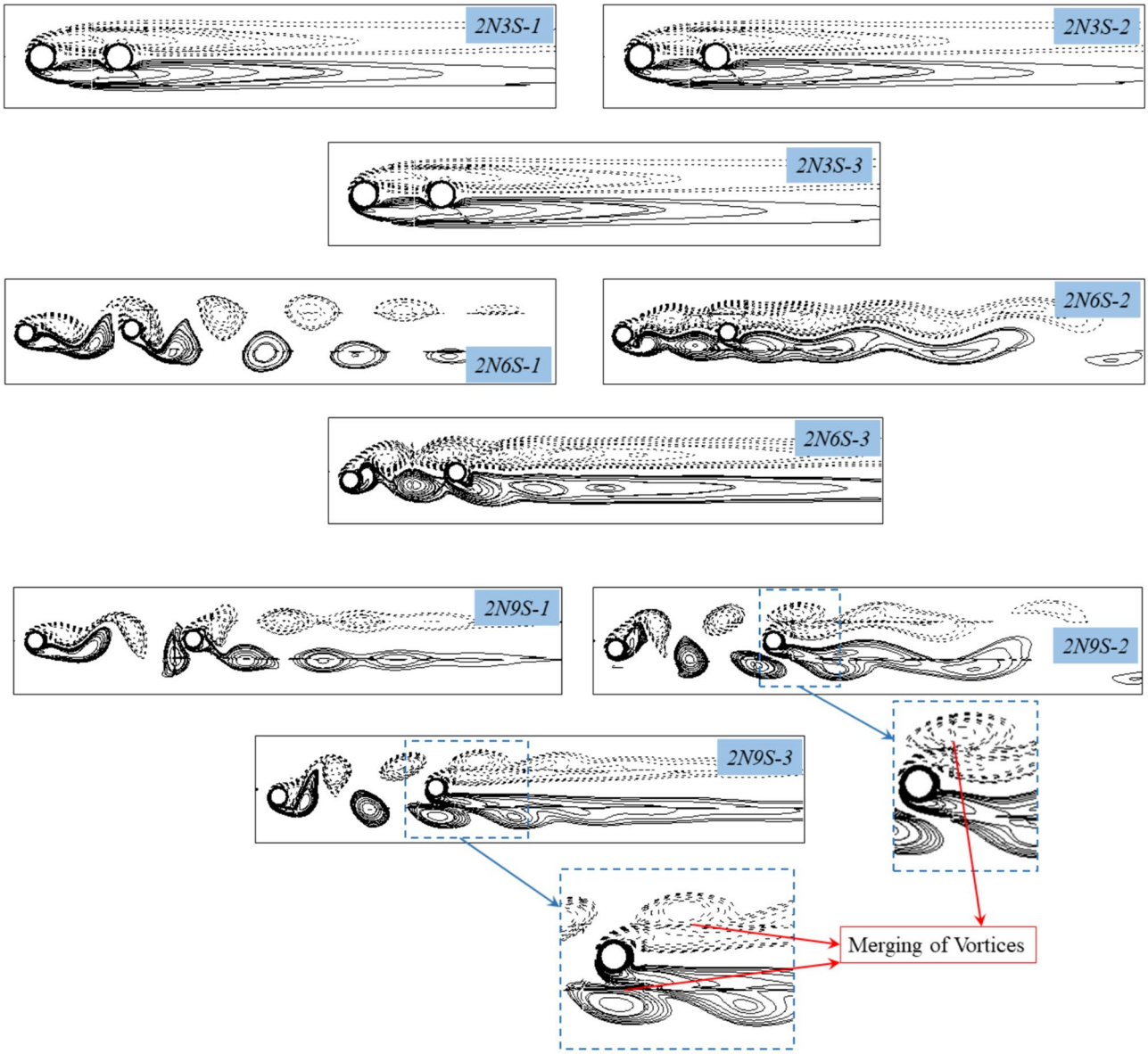


**Fig. 8** Instantaneous ($t.^{*}=250$) vorticity contour for different space and different structural combinations at $U_r=5$, $m^{*}=10$ and $Re=100$

Cyl-II is fixed, it can be seen that four wakes are formed behind the Cyl-I and one wake behind the Cyl-II. Although, only one wake is seen behind the Cyl-I when Cyl-III is fixed.

## Vortex Shedding Characteristics

In order to investigate the dynamics of the vibrating cylinder thoroughly, the instantaneous vortex structures ($t^{*}=250$) are shown in Figs. 8 and 9 for different values of $N=2$ and 4, respectively, at $m^{*}=10$, $\zeta=0$ and $Re=100$. For, $S^{*}=3$, two shear layers of the opposite magnitude separate from the top and bottom surfaces of the upstream cylinder and reattach on the downstream cylinder in a completely stable form (*2N3S-1, 2N3S-2* and *2N3S-3*). A steady flow region in between the two cylinders is observed. The space between the cylinders is less than the wavelength of vortex shedding, which restricts the formation of Vortex Street behind the upstream cylinder. The vortex formed behind the downstream cylinder is found to be elongated without a Vortex Street, as the vortex formed by the upstream cylinder supresses the vortices formed behind the downstream cylinder and thus becomes elongated. At $S^{*}=6$, typical characteristics of the vortex shedding are observed. Two different vortices shed per cycle of the oscillation are found separated from both cylinders when the upstream cylinder is static (*2N6S-1*).

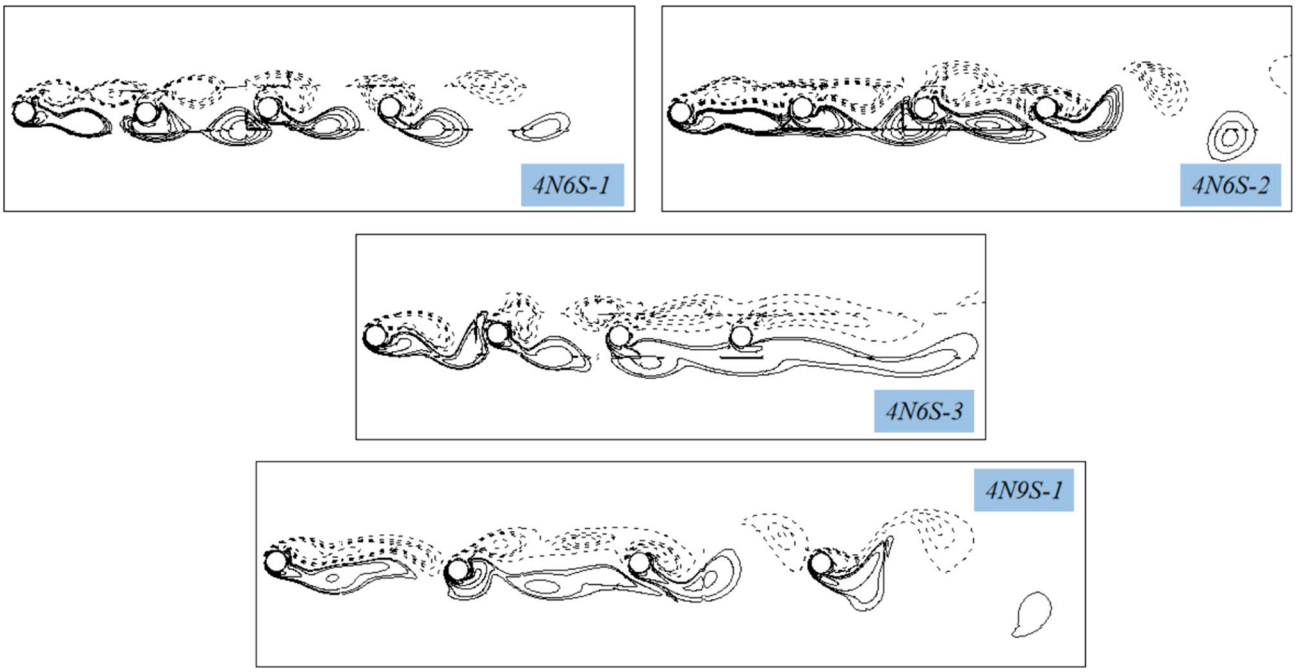


**Fig. 9** Instantaneous ($t^*=250$) vorticity pattern for different space and different structural combinations at $U_r=5$, $m.^*=10$ and $Re=100$ and $N=4$

However, when the upstream cylinder is freely vibrating, the shear layers are elongated longitudinally, irrespective, whether the downstream cylinder is static or vibrating. An asymmetric shear layers are observed where alternative reattachment takes place. These elongated shear layers develop instabilities. Further increment on the spacing to $S^*=9$, two different vortices are found separated from the cylinder surfaces; one is a clockwise rotating vortex separated from the bottom surfaces (continuous lines) and the other one is counter-clockwise rotating vortex detached from the top surfaces (dashed lines) when the upstream cylinder is static (refer to *2N9S-1*). However, when the downstream cylinder is in vibrating condition, the two separated vortices are shed per cycle of oscillation behind the upstream cylinder. The stretching of these vortices are found more when both cylinders are in the vibrating state (refer *2N9S-3*). At the instantaneous time, $t^*=250$, the merging of upstream vortices with the downstream one is observed (refer to inset views) and further advection occurs along the flow direction. As a result, a stretch in the vortices formed over the downstream cylinder is found.

Figure 9 depicts the instantaneous vortex flow pattern for $N=4$ at $t^*=250$, $U_r=5$, $m^*=10$ and $Re=100$. It can be noticed that the vortex pattern is highly dependent on the structural coalitions of the cylinders for $S^*=6$. When all the cylinders are allowed to vibrate at $S^*=6$ and 9 (*4N6S-1* and *4N9S-1*), two different vortices are found separated from all the cylinder surfaces; one is a clockwise rotating vortex separated from the bottom surfaces (continuous lines), and the other is counter-clockwise rotating vortex detached from the top surfaces (dashed lines). However, when the Cyl-II and Cyl-IV are in static condition at $S^*=6$, separation of the vortices is observed only from the Cyl-IV. The vortices from the other three cylinders are stretched and overlapped with the next vortices, resulting in the merging of the vortices. This merging of the vortices from the Cyl-II enhances the transverse movement of the Cyl-III (discussed later). Although, a distinct characteristic of the vortex is observed when Cyl-I and Cyl-III are in static conditions. There is no separation of the vortices behind the Cyl-III and the vortices are stretched enough to merge with the vortices around the Cyl-IV. Due to this, the cylinder experiences more vibration in the transverse direction.

## Flow-Induced Force

The energy that can be harvested from the VIV is related to the total force acting on a body in the transverse direction of the incoming fluid, *i.e.,* the lift force (refer to Eq. 8). Thus, the non-dimensional form of the maximum lift-force as the maximum lift-coefficient ($C_{L,max}$) for the different number of cylinders, spacing, and structural conditions of the cylinders is shown in Fig. 10a–c. In addition, $C_{L,max}$ developed from the other corresponding lower number of cylinders is also depicted in the Fig. 9 for a simple comparison.

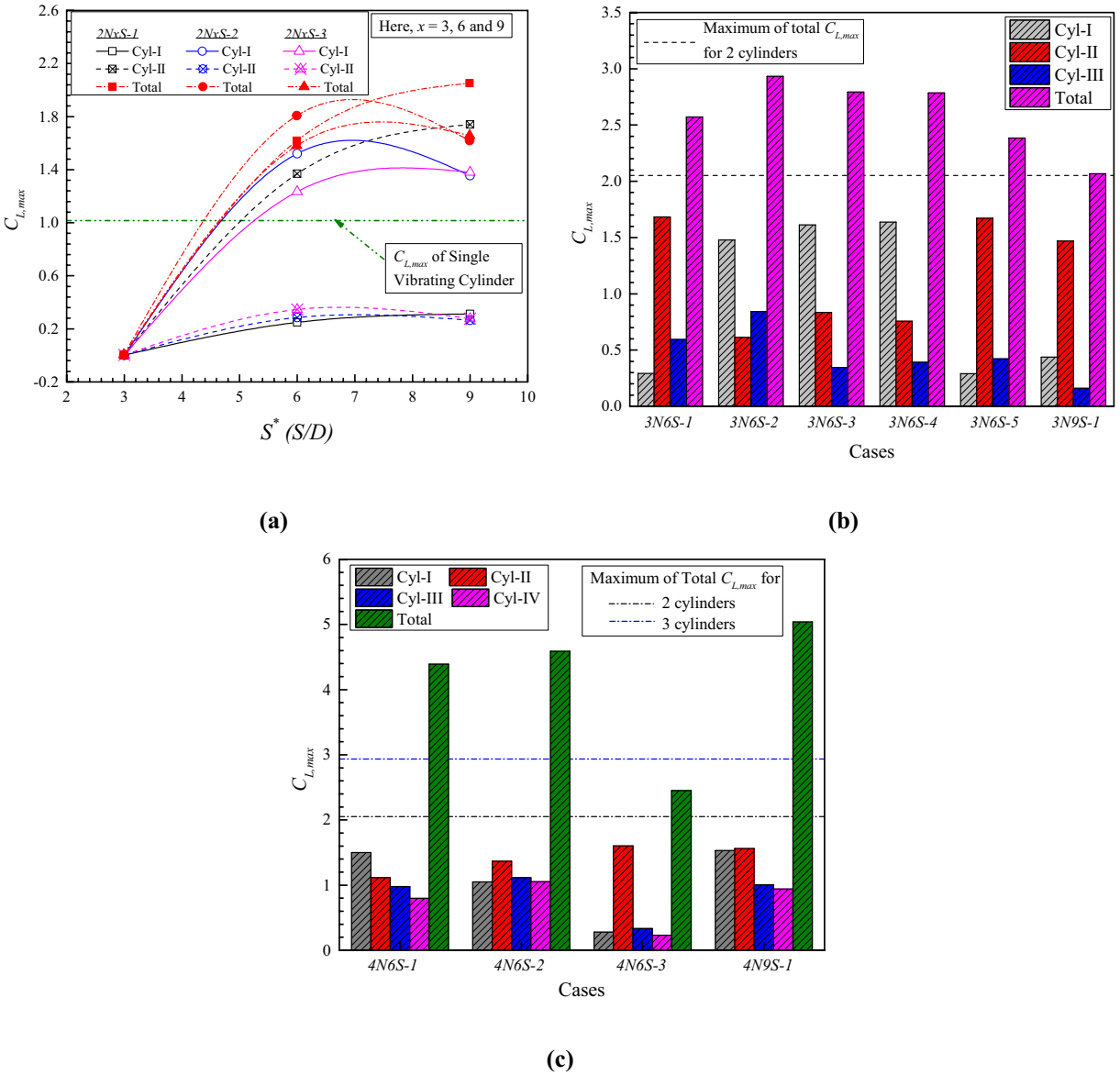


**Fig. 10** Variation of maximum lift-coefficient for cylinders in tandem of different structural conditions for different number of cylinders **a** $N=2$, **b** $N=3$, and **c** $N=4$

The lift force experienced by a cylinder in cross flow is mainly the result of the vortex shedding developed by the movement of the vortex from top to bottom and bottom to top surfaces of a body. The characteristics of $C_{L,max}$ of 2 cylinders is shown in Fig. 10a. As discussed earlier, no undulation is observed on the streamline $S^*=3$, thus no significant lift is developed at $S^*=3$. However, when the spacing becomes $S^*=6$ and 9, a noteworthy lift force is observed. Although, $C_{L,max}$ of the Cyl-I and Cyl-II is very much less than the $C_{L,max}$ of a single vibrating cylinder, irrespective of the structural conditions of the Cyl-I. It is found that the $C_{L,max}$ of Cyl-I is much higher compared to $C_{L,max}$ of a single vibrating cylinder for two cases of structural conditions, *2NxS-2* and *2NxS-3* at $S^*=6$ and 9. Whereas, the $C_{L,max}$ of the Cyl-II is greater than that of the single cylinder only in one case, *2NxS-2* for $S^*=6$ and 9. However, the total $C_{L,max}$ is always higher than the $C_{L,max}$ of a single vibrating cylinder, irrespective of the structural conditions at $S^*=6$ and 9.

The maximum lift-coefficient ($C_{L,max}$) for N = 3 and for the different spacing and different structural conditions is shown in Fig. 10b. It can be observed that the maximum $C_L$ exists either in the Cyl-I or in the Cyl-II depending on the structural conditions. When the Cyl-I is in static condition, it experiences maximum lift force. However, when the Cyl-I is allowed to vibrate freely, the maximum $C_L$ is found in the Cyl-II. In addition, $C_{L,max}$ developed from an arrangement

of the two cylinders is also depicted in Fig. 10b to compare the impact of the three cylinders on the lift-force. It is found that the total $C_L$ of 3 cylinders is always greater than the total maximum $C_L$ of the 2 vibrating cylinders when the spacing is $S^*=6$, and an insignificant difference is observed at $S^*=9$ (*3N9S-1*).

The variation of the lift force of each cylinder of $N=4$ for the different structural conditions is shown in Fig. 10c. The maximum of total $C_{L,max}$ for $N=2$ and 3 is also shown as a dotted line for a clear comparison. When all four cylinders are allowed to vibrate freely at $S^*==6$ (*4N6S-1*), $C_{L,max}$ is more in the Cyl-I and gradually decreases to the Cyl-IV as separation of the vortices is observed from each of the cylinders. Also, it is noticed that the strength of the vortices reduces gradually with spacing. However, when $S^*=9$, the $C_{L,max}$ is maximum and is equal in both the Cyl-I and II. For the other considered structural conditions, it is noticed that the $C_{L,max}$ is greater in the Cyl-II. It can also be observed that the total $C_{L,max}$ of the four cylinders is always more than the total $C_{L,max}$ of 2 and 3 cylinders. However, when Cyl-I and Cyl-III (*4N6S-3*) are in static condition, the total $C_{L,max}$ of the four cylinders is less than $C_{L,max}$ of the three cylinders.

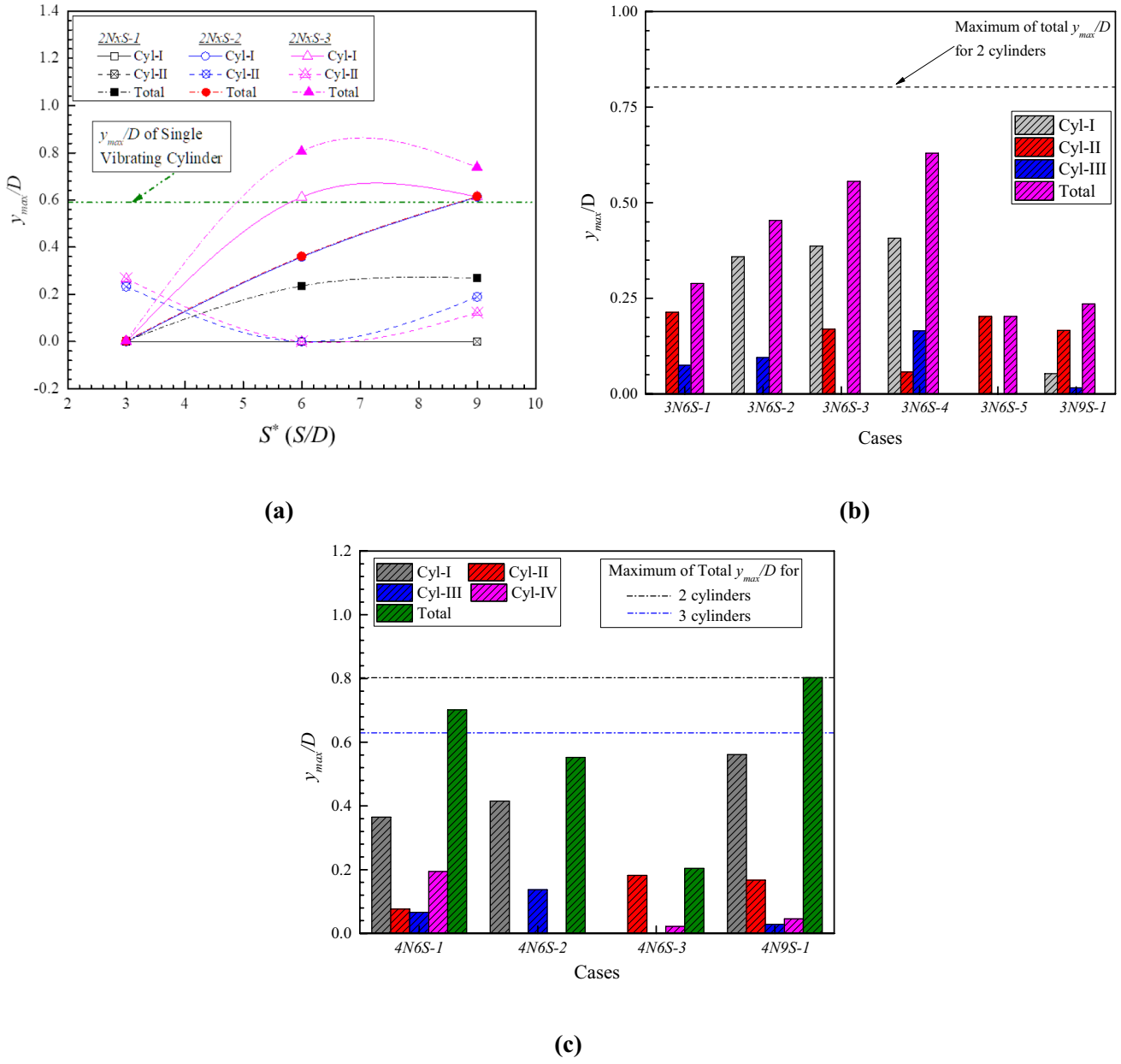


**Fig. 11** Variation of normalized maximum transverse displacement for cylinders in tandem of different structural conditions for different number of cylinders **a** $N=2$, **b** $N=3$, and **c** $N=4$

## Normalized Maximum Transverse Displacement

The maximum amplitude of the cylinder vibration is one of the crucial aspects that can effectively quantify the VIV and is shown in Fig. 11a–c for $N=2$, 3 and 4 for different cylinder spacing and structural conditions. The maximum amplitude of the cylinder vibration is normalized by using the cylinder diameter as $y_{max}/D$. Here, the zero value of $y_{max}/D$ for a particular cylinder implies the static condition is applied to that cylinder. Figure 11a depicts the variation of $y_{max}/D$ for $N=2$ and it is observed that $y_{max}/D$ is much lower than the $y_{max}/D$ of a single vibrating cylinder for the two structural conditions, *2NxS-1* and *2NxS-2*, at $S^*=3$ and 6. However, when the upstream cylinder is allowed to vibrate freely, $y_{max}/D$ is always higher than the $y_{max}/D$ of a single vibrating cylinder at $S^*=6$ and 9. The strength of vortices is higher when the spacing is greater than 3D, as discussed earlier, and these vortices push the vibrating cylinders more in the transverse direction of the flow.

The variation of the maximum value of the normalized transverse displacement for $N=3$ is shown in Fig. 11b for the different cylinder spacing and structural conditions. It is observed that the $y_{max}/D$ of the three cylinders is much lower than the $y_{max}/D$ of the two cylinders, irrespective of the spacing and structural conditions. This is due to the lesser strength of the vortices around the three cylinders arrangement than the vortices around the two cylinders, and the movement of the vibrating cylinders in the transverse direction of the flow is directly proportional to this strength of the vortices. The maximum value of $y_{max}/D$ is found as 0.41 in Cyl-I at $S^*=6$ when all three cylinders are in vibrating condition.

Figure 11c shows the characteristics of the maximum amplitude of the normalized transverse displacement of the vibrating cylinders of $N=4$ for different non-dimensional spacing and structural conditions. A simple comparison of the maximum of total $y_{max}/D$ between the two, three, and four cylinders is also depicted. At $S^*=6$ and 9, $y_{max}/D$ is more in the Cyl-I when it is allowed to vibrate freely. Thus, the transverse displacement is significantly dependent on the $S^*$. When $S^*$ is greater than 6, the contact of vortices with the Cyl-I is more intense, resulting in more transverse displacement. It is observed that the total $y_{max}/D$ of the four cylinders is greater than the $y_{max}/D$ of the three cylinders in two cases, *4N6S-1* and *4N9S-1*. However, the four cylinder arrangement is found to be more effective than the two and three cylinder arrangement in terms of total $y_{max}/D$ only when $S^*=9$.

## Frequency of Oscillation and Power Generation

Figure 12 illustrates the characteristic of the non-dimensional frequency of transverse oscillation, $f^*$ ($f_{cycle}/f_n$) of VIV with varying $S^*$, and the number of cylinders arranged in tandem. Here, $f_{cycle}$ is the total frequency of transverse

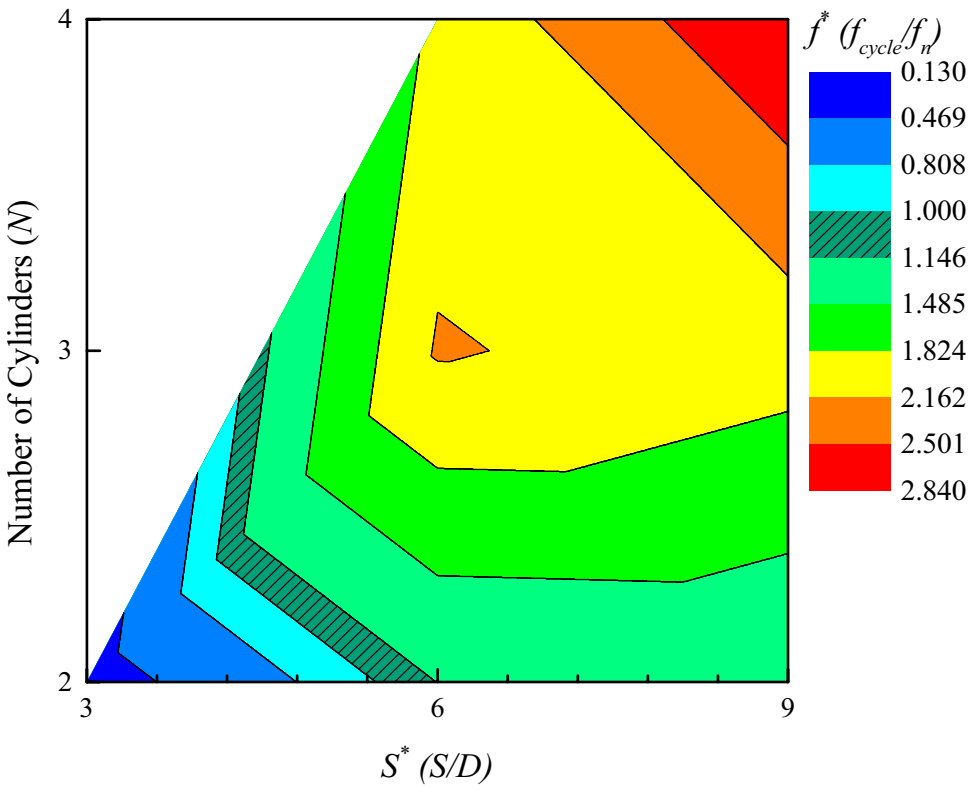


**Fig. 12** Dependency of non-dimensional frequency of transverse oscillation on $S^*$ and number of cylinders

oscillation of all cylinders. A lock-in region can be observed where the frequency of oscillation is equal to the frequency of vortex shedding, i.*e.*, $f^* = 1$. This lock-in region is noticed for different structural conditions considered in the present study and for the number of cylinders 2 and 3 at space, $S^* \leq 6$. It increases with a decreasing number of cylinders, and space between the cylinders along with the structural conditions imposed on the cylinders. It can also be noticed that when the space and number of cylinders is greater, the $f^*$ reaches its maximum value of 2.840 for all the considered cases. As discussed earlier, the separation of vortices takes place in a very short time, and with higher strength, when the space is larger with more number of cylinders arranged in tandem.

The impacts of two significant parameters, viz., the number of cylinders arranged in tandem ($N$) and the non-dimensional spacing between the cylinders ($S^*$) on the power developed by VIV are profoundly examined and shown as a three-dimensional contour in Fig. 13. The contour plot in Fig. 13 shows the dependency of harvested power for different spacing values, and numbers of tandem circular cylinders when the other parameters are kept constant as $U_r = 5$, $m^* = 10$ and $Re = 100$. It is noticed that the harvested energy from VIV ($Power_{VIV}$) is significantly dependent on $S^*$ and $N$ for all the considered cases. The value of harvested power from the single cylinder is not shown in the contour, however, it is very important for the comparison with the multiple cylinder arrangement. The maximum value of $Power_{VIV}$ is found as 2.5 mW for the single cylinder arrangement at $U_r = 5$. For multiple cylinders,$Power_{VIV}$ is found to increase with increasing of both the $S^*$ and $N$. A maximum $Power_{VIV}$ of 10.55 mW is developed for four cylinders arranged in tandem at a non-dimensional distance, $S^* = 9$, when all the cylinders are allowed to vibrate freely. As discussed earlier, an increase in the spacing is followed by an increase in the natural frequency of the energy harvester (refer to Fig. 12). In addition, it is clear that the vibration amplitude of the cylinder in the lock-in region is increased, and hence the output power is enhanced with the increase in spacing distance [16]**.** Besides, greater strength of vortices are formed with an increasing number of cylinders and space and strike the cylinders with more force, resulting in a higher lift force. As a result, more power is developed at higher $S^*$ and $N$.

The VIV power is in relation to the frequency (see Eq. 8 and 9). Therefore, the vibrational frequency has a great effect on the VIV power. The influence of the non-dimensional frequency of transverse displacement ($f^*$) of cylinders on the $Power_{VIV}$ along with the space between the cylinders is depicted in Fig. 14. As discussed earlier, the $f^*$ increases with the increasing of both parameters, the number of cylinders and non-dimensional space, $Power_{VIV}$ is also found to be increased with the increment of $f^*$. The local average velocity of flow at downstream increases

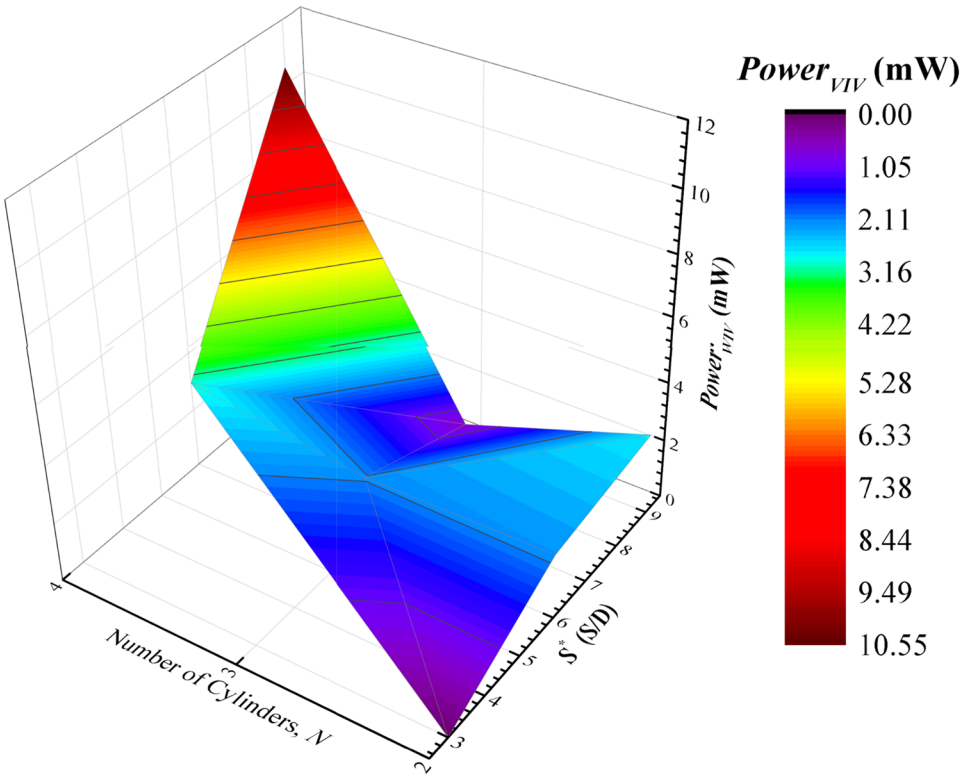


**Fig. 13** Dependency of $Power_{VIV}$ on $S^*$ and number of cylinders, $N$

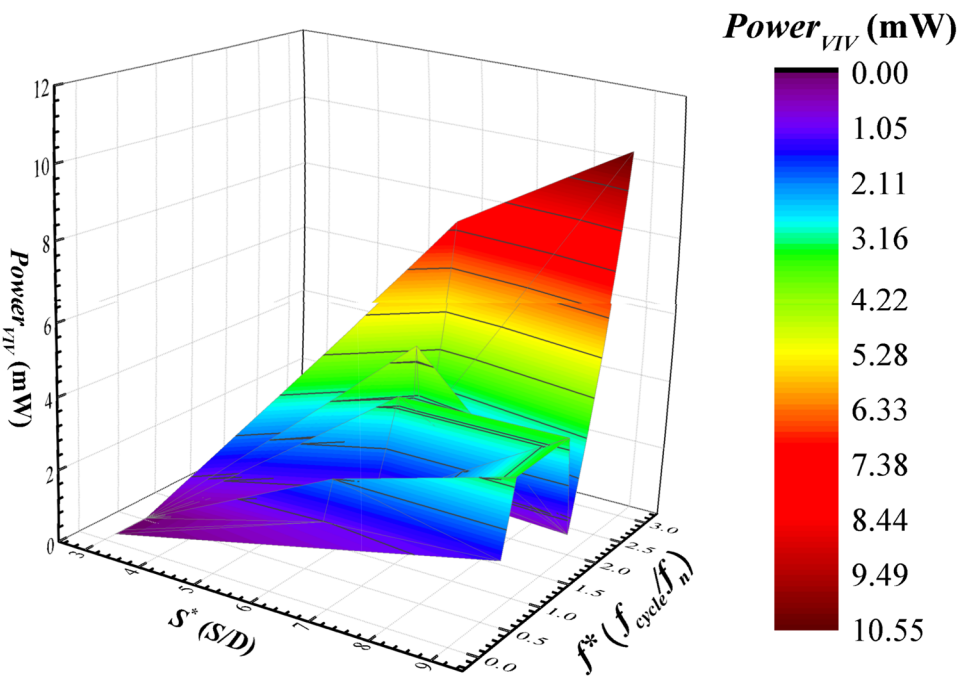


**Fig. 14** Dependency of $Power_{VIV}$ on $S^*$ and $f^*$

when cylinders are kept at downstream, resulting in disturbance in the flow which is significantly influenced by the number of cylinders, the space between them, and most importantly, the structural conditions of the cylinders arranged in tandem. In particular, due to slower flow separation (image not included), the frequency of the cylinders is obviously low for the few cases considered in the present study. However, the total frequencies of the cylinders increase with $S^*$, resulting in more $Power_{VIV}$. Again, it can be seen that when the spacing ratio, $S^*$ is small ($S^* < 6$), a blocking effect is apparent (refer to Fig. 6). Thus, insignificant power is developed at very low space.

## Efficiency of Total Energy Conversion, $\eta_{VIV}$

The dependency of harvested power from VIV on the number of cylinders arranged in tandem, spacing ratio, and non-dimensional frequency is discussed. It is noticed that the discussed parameters have a significant effect on the $Power_{VIV}$. The harvested power increases with an increasing spacing ratio ($S^*$) and number of cylinders ($N$). However, the efficiency of power harvesting may have a different kinds of dependencies. Thus, the dependence of VIV efficiency, $\eta_{VIV}$ (Eq. 11) on the number of cylinders arranged in tandem ($N$), and spacing ratio ($S^*$) for different combinations of structural conditions is shown in Fig. 15. For a single cylinder, a maximum value of 0.58 of $\eta_{VIV}$ is found, and a straight line is drawn for comparison with the multiple cylinder arrangement, irrespective of the spacing ratio. The maximum efficiency is achieved at $U_r = 5$ for $N = 1$. When the number of cylinders increased to 2

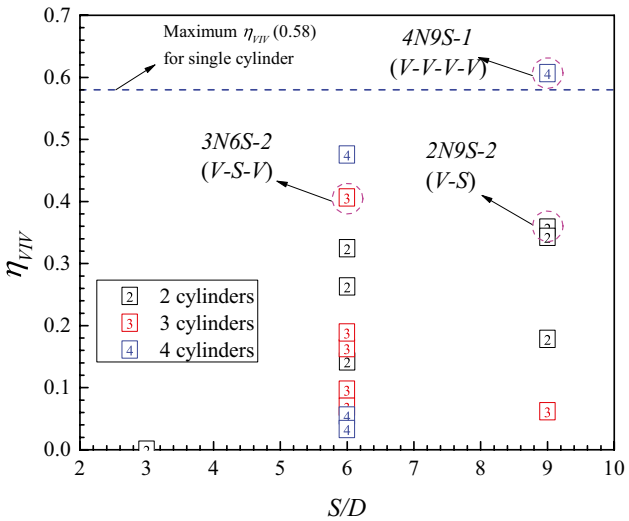


**Fig. 15** Characteristic of efficiency of total energy conversion, $\eta_{VIV}$ with spacing ratio and number of cylinders

for $S^* = 3$, insignificant VIV efficiency is observed. However, at $S^* = 6$, the minimum and maximum efficiencies are noticed for $N = 4$, and the values are 0.03, and 0.47, respectively. When $S^*$ increases to 9, minimum and maximum efficiencies are found for $N = 3$ and 4, respectively. The corresponding minimum and maximum values of $\eta_{VIV}$ are 0.06 and 0.61, respectively. From all the considered cases, the maximum value of $\eta_{VIV} = 0.61$ is achieved for $N = 4$ and at $S^* = 9$ when all the cylinders are allowed to vibrate freely. The maximum value of $\eta_{VIV}$ is observed as 0.36 at $S^* = 9$ for $N = 2$. Whereas, the maximum value of

$\eta_{VIV}$ is 0.41 for $N=3$ at $S^*=6$. The corresponding cases are highlighted in Fig. 15, which are *2N9S-2* (*V-S*), *3N6S-2* (*V-S-V*), and *4N9S-1* (*V-V-V-V*) for $N=2$, 3, and 4, respectively. The letters in the parenthesis denote the structural condition of the cylinders arranged in tandem in the direction of flow accordingly. The value of $\eta_{VIV}$ (maximum is 0.61) in the present investigation can be found to be insignificant. However, a maximum value of harvested power efficiency is found as 0.52 in the earlier studies where the corresponding Reynolds number is of order $10^4$ [2, 51, 54], whereas the Reynolds number in the present study is kept as very low as 100. The efficiency can be enhanced by increasing the wind velocity, which ultimately increases the *Re* and also by increasing the number of cylinders and number of piezoelectric strips, as depicted in Fig. 2. Although, the number of piezoelectric strips cannot be increased arbitrarily as it increases the overall mass of the arrangement, which will further reduce the vibrational frequency. Thus, a trade-off between the harvested power and efficiency needs to be investigated for achieving optimized harvested power from the VIV by using multiple cylinders arranged in tandem.

## Conclusions

A numerical analysis of vortex induced vibration of single and multiple circular cylinders arranged in tandem for a constant Reynolds number, $Re=100$, is reported in the present study. The number of cylinders in a multiple cylinder arrangement is varied by 2, 3, and 4 along with a single cylinder arrangement. The spacing between adjacent cylinders varies as 3*D*, 6*D* and 9*D*; where *D* is the cylinder diameter and a combination of structural conditions; static and freely vibrating are also considered at the same time. The effects of spacing, structural combination, and number of cylinders on flow characteristics, fluid forces, transverse displacement, and energy harvested from VIV are studied, and the following conclusions are drawn.

1. For a single vibrating cylinder, primary wake, primary wake with secondary wake, and no wake is observed for different $U_r$. Whereas, the wake is noticed to be wavy when $N=2$, 3, and 4 at $S^*=6$, and 9, resulting in vortex shedding irrespective of the structural conditions. A very unique characteristic of the vorticity pattern of single to four vortices is observed between Cyl-I and Cyl-II for $N=4$ at different values of $S^*$.
2. The maximum lift-force is found to be dependent on both the spacing and the structural condition. The values of $C_{L,max}$ are 1.02, 1.74, 1.68, and 1.60 for $N=1$, 2, 3, and 4, respectively. The corresponding structural conditions are *S-V*, *S-V-V*, and *S-V-S-V* when $N=2$, 3, and 4 at $S^*=9$, 6, and 6, respectively. Whereas, the maximum transverse displacement is found as $y_{max}/D=0.59$, 0.62, 0.41, and 0.56 when $N=1$, 2, 3, and 4, respectively. The transverse displacement is maximum when all the cylinders are allowed to vibrate freely in multi-cylinder cases.
3. The energy harvested from VIV, ($Power_{VIV}$) is significantly dependent on $S^*$, *N*, and the frequency of transverse oscillation, $f^*$ ($f_{cycle}/f_n$). A maximum value of $Power_{VIV}$ of 10.55 mW is achieved for the maximum values of $S^*=9$, $N=4$, and $f^*=2.84$. The corresponding maximum value of $\eta_{VIV}$ is achieved as 0.61 for $N=4$ and at $S^*=9$ when all the cylinders are allowed to vibrate freely.

However, when $N=3$, $\eta_{VIV}$ is maximum at $S^*=6$ instead of $S^*=9$. Although, $\eta_{VIV}$ is maximum at $S^*=9$ for $N=2$. Thus, an increase in number of cylinders does not always enhance the energy conversion efficiency, as the efficiency is highly dependent on the spacing between the cylinders. It can also be concluded that the harvested output power can be multiplied by increasing the number of piezoelectric strips, as discussed earlier (refer to Fig. 2). Although, the overall mass of the arrangement is then increased that needs to be optimized to achieve maximum lift force, transverse displacement, and frequency of oscillation.

The present results provide knowledge on the application of a set of tandem cylinders combining with vibrational mode for harvesting the power from VIV in a practically engineered nano/micro energy harvesting system, as demanded by the specific application on hand.

**Supplementary Information** The online version contains supplementary material available at https://doi.org/10.1007/s42417-024-01408-x.

**Acknowledgements** The financial supports for this research provided by the SCIENCE & ENGINEERING RESEARCH BOARD (SERB), a statutory body of the Department of Science & Technology, Government of India, (Grant No. SRG/2021/000778) is gratefully acknowledged.

**Funding** The funding has been received from Science and Engineering Research Board with Grant no. SRG/2021/000778.

**Data Availability** Data supporting the findings of this study are included within the article.

## Declarations

**Conflict of Interest** The author reports no conflict of interest.

## References

1. Magagna D, Uihlein A (2015) Ocean energy development in Europe: Current status and future perspectives, International Journal of Marine. Energy 11:84–104

2. Zhu H, Gao Y (2018) Hydrokinetic energy harvesting from flow-induced vibration of a circular cylinder with two symmetrical fin-shaped strips. Energy 165:1259–1281
3. Zhou S, Wang J (2018) Dual serial vortex-induced energy harvesting system for enhanced energy harvesting. AIP Adv 8:075221
4. Zhang M, Zhao G, Wang J (2017) Study on fluid-induced vibration power harvesting of square columns under different attack angles. Geofluids. https://doi.org/10.1155/2017/6439401
5. Abdelkefi A (2016) Aeroelastic energy harvesting: a review. Int J Eng Sci 100:112–135
6. Nabavi S, Zhang L (2016) Portable wind energy harvesters for low-power applications: a survey. Sensors 16:1101
7. Zhao L, Yang Y (2017) Toward small-scale wind energy harvesting: design, enhancement, performance comparison, and applicability. Shock Vib. https://doi.org/10.1155/2017/3585972
8. Seyed-Aghazadeh B, Samandari H, Dulac S (2020) Flow-induced vibration of inherently nonlinear structures with applications in energy harvesting. Phys Fluids 32:071701
9. El-Bary A (2005) Exponential solution of a problem of two-dimensional motion of micropolar fluid in a half-plane. J Appl Math Comput 165:81–93
10. El-Bary A (2005) Computational treatment of free convection effects on perfectly conducting viscoelastic fluid. J Appl Math Comput 170:801–820
11. Ezzat M, El-Bary A (2016) Effects of variable thermal conductivity on Stokes' flow of a thermoelectric fluid with fractional order of heat transfer. J Int J Thermal Sci 100:305–315
12. Ezzat M, El-Bary A, Ezzat S (2011) Combined heat and mass transfer for unsteady MHD flow of perfect conducting micropolar fluid with thermal relaxation. J Energy Conver Manag 52:934–945
13. Ezzat M, El-Karamany A, El-Bary A (2015) On thermo-viscoelasticity with variable thermal conductivity and fractional-order heat transfer. J Int J Thermophys 36:1684–1697
14. Ezzat MA, El-Bary AA (2016) Thermoelectric MHD with memory-dependent derivative heat transfer. J Int Commun Heat Mass Transfer 75:270–281
15. Dai HL, Abdelkefi A, Yang Y, Wang L (2016) Orientation of bluff body for designing efficient energy harvesters from vortex-induced vibrations. Appl Phys Lett 108:053902
16. Naseer R, Dai H, Abdelkefi A, Wang L (2017) Piezomagnetoelastic energy harvesting from vortex-induced vibrations using monostable characteristics. Appl Energy 203:142–153
17. Liu F-R, Zhang W-M, Zhao L-C, Zou H-X, Tan T, Peng Z-K, Meng G (2020) Performance enhancement of wind energy harvester utilizing wake flow induced by double upstream flat-plates. Appl Energy 257:114034
18. Sun W, Zhao D, Tan T, Yan Z, Guo P, Luo X (2019) Low velocity water flow energy harvesting using vortex induced vibration and galloping. Appl Energy 251:113392
19. Soti AK, De A (2020) Vortex-induced vibrations of a confined circular cylinder for efficient flow power extraction. Phys Fluids 32:033603
20. Bernitsas MM, Raghavan K, Ben-Simon Y, Garcia E (2008) VIVACE (vortex induced vibration aquatic clean energy): a new concept in generation of clean and renewable energy from fluid flow. J Offshore Mech Arctic Eng 130.
21. Zhang L, Dai H, Abdelkefi A, Wang LJE (2019) Experimental investigation of aerodynamic energy harvester with different interference cylinder cross-sections. Energy 167:970–981
22. Ding L, Zhang L, Bernitsas MM, Chang C-C (2016) Numerical simulation and experimental validation for energy harvesting of single-cylinder VIVACE converter with passive turbulence control. Renewable Energy 85:1246–1259
23. Ding L, Zou Q, Zhang L, Wang H (2018) Research on flow-induced vibration and energy harvesting of three circular cylinders with roughness strips in tandem. Energies 11:2977
24. Zou Q, Ding L, Wang H, Wang J, Zhang L (2019) Two-degree-of-freedom flow-induced vibration of a rotating circular cylinder. Ocean Eng 191:106505
25. Sharpes N, Abdelkefi A, Hajj M, Heo J, Cho K-H, Priya S (2015) Preloaded freeplay wide-bandwidth low-frequency piezoelectric harvesters. Appl Phys Lett 107:023902
26. Hu G, Wang J, Su Z, Li G, Peng H, Kwok K (2019) Performance evaluation of twin piezoelectric wind energy harvesters under mutual interference. Appl Phys Lett 115:073901
27. Dai H, Abdelkefi A, Javed U, Wang L (2015) Modeling and performance of electromagnetic energy harvesting from galloping oscillations. Smart Mater Struct 24:045012
28. Naifar S, Bradai S, Viehweger C, Kanoun O (2017) Survey of electromagnetic and magnetoelectric vibration energy harvesters for low frequency excitation. Measurement 106:251–263
29. Soti AK, Thompson MC, Sheridan J, Bhardwaj R (2017) Harnessing electrical power from vortex-induced vibration of a circular cylinder. J Fluids Struct 70:360–373
30. Basset P, Galayko D, Paracha AM, Marty F, Dudka A, Bourouina T (2009) A batch-fabricated and electret-free silicon electrostatic vibration energy harvester. J Micromech Microeng 19:115025
31. Hoffmann D, Folkmer B, Manoli Y (2009) Fabrication, characterization and modelling of electrostatic micro-generators. J Micromech Microeng 19:094001
32. Zhang L, Dai H, Abdelkefi A, Wang L (2019) Experimental investigation of aerodynamic energy harvester with different interference cylinder cross-sections. Energy 167:970–981
33. Bibo A, Alhadidi AH, Daqaq MF (2015) Exploiting a nonlinear restoring force to improve the performance of flow energy harvesters. J Appl Phys 117:045103
34. Dai H, Abdelkefi A, Wang L (2014) Theoretical modeling and nonlinear analysis of piezoelectric energy harvesting from vortex-induced vibrations. J Intell Mater Syst Struct 25:1861–1874
35. Soti AK, Zhao J, Thompson MC, Sheridan J, Bhardwaj R (2018) Damping effects on vortex-induced vibration of a circular cylinder and implications for power extraction. J Fluids Struct 81:289–308
36. Mehmood A, Abdelkefi A, Hajj M, Nayfeh A, Akhtar I, Nuhait A (2013) Piezoelectric energy harvesting from vortex-induced vibrations of circular cylinder. J Sound Vib 332:4656–4667
37. Hu G, Tse K-T, Kwok KC, Song J, Lyu Y (2016) Aerodynamic modification to a circular cylinder to enhance the piezoelectric wind energy harvesting. Appl Phys Lett 109:193902
38. Zhang B, Song B, Mao Z, Tian W, Li BJE (2017) Numerical investigation on VIV energy harvesting of bluff bodies with different cross sections in tandem arrangement. Energy 133:723–736
39. Kim ES, Bernitsas MM (2016) Performance prediction of horizontal hydrokinetic energy converter using multiple-cylinder synergy in flow induced motion. Appl Energy 170:92–100
40. Zhang B, Mao Z, Song B, Tian W, Ding W (2018) Numerical investigation on VIV energy harvesting of four cylinders in close staggered formation. Ocean Eng 165:55–68
41. Zhang B, Song B, Mao Z, Tian W, Li B (2017) Numerical investigation on VIV energy harvesting of bluff bodies with different cross sections in tandem arrangement. Energy 133:723–736
42. Meneghini JR, Saltara F, Siqueira CDLR, Ferrari JJJOF Jr (2001) Structures, numerical simulation of flow interference between two circular cylinders in tandem and side-by-side arrangements. J Fluids Struct 15:327–350
43. Jung SY, Kim JJ, Park HW, Lee SJ (2018) Comparison of flow structures behind rigid and flexible finite cylinders. Int J Mech Sci 142:480–490
44. Sun W, Hu S, Li H, Chen R, Zhao DJIJOMS (2024) Enhancement of piezoelectric energy harvesting by the elliptical cylinder interference. Int J Mech Sci 263:108785

45. Hobbs WB, Hu DL (2012) Tree-inspired piezoelectric energy harvesting. J Fluids Struct 28:103–114
46. Shan X, Song R, Fan M, Xie T (2016) Energy-harvesting performances of two tandem piezoelectric energy harvesters with cylinders in water. Appl Sci 6:230
47. Zhang L, Dai H, Abdelkefi A, Wang L (2017) Improving the performance of aeroelastic energy harvesters by an interference cylinder. Appl Phys Lett 111:073904
48. Sun H, Ma C, Kim ES, Nowakowski G, Mauer E, Bernitsas MM (2017) Hydrokinetic energy conversion by two rough tandem-cylinders in flow induced motions: effect of spacing and stiffness. Renew Energy 107:61–80
49. Hu G, Liu F, Li L, Li C, Xiao Y, Kwok K (2019) Wind energy harvesting performance of tandem circular cylinders with triangular protrusions. J Fluids Struct 91:102780
50. Han P, Pan G, Zhang B, Wang W, Tian W (2020) Three-cylinder oscillator under flow: flow induced vibration and energy harvesting. Ocean Eng 211:107619
51. Chen Z, Alam MM, Qin B, Zhou Y (2020) Energy harvesting from and vibration response of different diameter cylinders. Appl Energy 278:115737
52. Tamimi V, Wu J, Naeeni S, Shahvaghar-Asl S (2021) Effects of dissimilar wakes on energy harvesting of flow induced vibration (FIV) based converters with circular oscillator. Appl Energy 281:116092
53. Sen S, Mittal S (2015) Effect of mass ratio on free vibrations of a square cylinder at low Reynolds numbers. J Fluids Struct 54:661–678
54. Zhang B, Wang K-H, Song B, Mao Z, Tian W (2018) Numerical investigation on the effect of the cross-sectional aspect ratio of a rectangular cylinder in FIM on hydrokinetic energy conversion. Energy 165:949–964
55. Prasanth T, Mittal S (2008) Vortex-induced vibrations of a circular cylinder at low Reynolds numbers. J Fluid Mech 594:463–491
56. Bourguet R (2019) Flow-induced vibrations of a rotating cylinder in an arbitrary direction. J Fluid Mech 860:739–766
57. Patankar SV (1980) Numerical heat transfer and fluid flow. Hemisphere Publishing Corporation, New York, p 58
58. Bhatt R, Alam MM (2018) Vibrations of a square cylinder submerged in a wake. J Fluid Mech 853:301–332
59. Singh S, Mittal S (2005) Vortex-induced oscillations at low Reynolds numbers: hysteresis and vortex-shedding modes. J Fluids Struct 20:1085–1104
60. Zhao M, Cheng L, Zhou T (2013) Numerical simulation of vortex-induced vibration of a square cylinder at a low Reynolds number. Phys Fluids 25:023603
61. Kumar D, Sourav K, Sen S (2019) Steady separated flow around a pair of identical square cylinders in tandem array at low Reynolds numbers. Comput Fluids 191:104244